



HAL
open science

Effects of wind speed and atmospheric stability on the air pollution reduction rate induced by noise barriers

Nicolas Reiminger, Xavier Jurado, José Vazquez, Cédric Wemmert, Nadège Blond, Matthieu Dufresne, Jonathan Wertel

► To cite this version:

Nicolas Reiminger, Xavier Jurado, José Vazquez, Cédric Wemmert, Nadège Blond, et al.. Effects of wind speed and atmospheric stability on the air pollution reduction rate induced by noise barriers. *Journal of Wind Engineering and Industrial Aerodynamics*, 2020, 200, pp.104160. 10.1016/j.jweia.2020.104160 . hal-03041494v1

HAL Id: hal-03041494

<https://hal.science/hal-03041494v1>

Submitted on 4 Dec 2020 (v1), last revised 5 Nov 2021 (v2)

HAL is a multi-disciplinary open access archive for the deposit and dissemination of scientific research documents, whether they are published or not. The documents may come from teaching and research institutions in France or abroad, or from public or private research centers.

L'archive ouverte pluridisciplinaire **HAL**, est destinée au dépôt et à la diffusion de documents scientifiques de niveau recherche, publiés ou non, émanant des établissements d'enseignement et de recherche français ou étrangers, des laboratoires publics ou privés.

See discussions, stats, and author profiles for this publication at: <https://www.researchgate.net/publication/340233360>

Effects of wind speed and atmospheric stability on the air pollution reduction rate induced by noise barriers

Article in *Journal of Wind Engineering and Industrial Aerodynamics* · March 2020

DOI: 10.1016/j.jweia.2020.104160

CITATIONS

0

READS

32

7 authors, including:



Nicolas Reiminger

ICube Laboratory

6 PUBLICATIONS 2 CITATIONS

[SEE PROFILE](#)



Xavier Jurado

ICube Laboratory

3 PUBLICATIONS 1 CITATION

[SEE PROFILE](#)



José Vazquez

Ecole Nationale du Génie de l'Eau et de l'Environnement de Strasbourg

131 PUBLICATIONS 548 CITATIONS

[SEE PROFILE](#)



Cédric Wemmert

University of Strasbourg

83 PUBLICATIONS 807 CITATIONS

[SEE PROFILE](#)

Some of the authors of this publication are also working on these related projects:



COCLICO (ANR Project) [View project](#)



Smart Meter Inclusive (SMI): artificial intelligence to support the proactive management of energy consumption by end consumers [View project](#)

1 **Effects of wind speed and atmospheric stability on the air pollution reduction rate** 2 **induced by noise barriers**

3 Nicolas Reiminger^{1,2*}, Xavier Jurado^{1,2}, José Vazquez², Cédric Wemmert², Nadège Blond³,
4 Matthieu Dufresne¹, Jonathan Wertel¹

5 ¹*AIR&D, 67000, Strasbourg, France*

6 ²*ICUBE Laboratory, CNRS/University of Strasbourg, 67000, Strasbourg, France*

7 ³*LIVE Laboratory, CNRS/University of Strasbourg, 67000, Strasbourg, France*

8 **Corresponding author: Tel. +33 (0)6 31 26 75 88, Mail. nreiminger@air-d.fr*

9

10 Please cite this paper as : Reiminger, N., Jurado, X., Vazquez, J., Wemmert, C., Blond, N., Dufresne,
11 M., Wertel, J., 2020. Effects of wind speed and atmospheric stability on the air pollution reduction rate
12 induced by noise barriers. Journal of Wind Engineering and Industrial Aerodynamics 200, 104160.
13 <https://doi.org/10.1016/j.jweia.2020.104160>

14

15 **ABSTRACT**

16 People around the world increasingly live in urban areas where traffic-related emissions can
17 reach high levels, especially near heavy-traffic roads. It is therefore necessary to find short-term
18 measures to limit the exposure of this population and noise barriers have shown great potential
19 for achieving this. Nevertheless, further work is needed to better understand how they can act
20 on pollution reduction. To do this, a Reynolds-Averaged Navier-Stokes model that takes into
21 account thermal effects is used to study the effects of wind speed and atmospheric stability on
22 the concentration reduction rates (*CRR*) induced by noise barriers. This study shows that the
23 *CRR* behind the barriers may depend on both wind and thermal conditions. Although only the
24 wind direction, and not the wind speed, has an impact on *CRR* in a neutral atmosphere, this
25 parameter can be changed by both wind speed and thermal variations in non-neutral
26 atmospheres. Stable cases lead to a higher *CRR* compared to unstable cases, while the neutral
27 case gives intermediate results. Finally, it is shown that the variation of *CRR* is negligible for
28 Richardson numbers ranging from -0.50 to 0.17.

29 **Keywords:** Computational fluid dynamics, Noise barrier, Air pollution, Wind speed, Thermal
30 stratification

31 **1. Introduction**

32 Nowadays, more than one in two people live in urban areas with 82% in the United States and
33 74% in Europe, and this percentage will continue growing to reach 68% worldwide in 2050
34 (United Nations, Department of Economic and Social Affairs, Population Division, 2019).
35 Traffic-related emissions can reach high levels in such areas, particularly near heavy-traffic
36 roads. Concentrations of air pollutants such as nitrogen dioxide (NO₂) and particulate matter
37 (PM) can reach high values in the vicinity of this kind of road and lead to several diseases
38 (Anderson et al., 2012; Kagawa, 1985; Kim et al., 2015). In addition, it has been shown that
39 people living near these roads are more likely to be at risk (Chen et al., 2017; Finkelstein et al.,
40 2004; Petters et al., 2004). In Europe, emissions and therefore concentrations of air pollutants
41 are expected to decrease in the future as air quality regulations increase and actions are taken
42 (European Commission, 2013). Nevertheless, it will take time to achieve a significant decrease
43 and, in the meantime, many people will still live in areas where air quality is poor. It is now
44 necessary to find ways to limit exposure to air pollution for people living near busy roads and
45 to better understand solutions that have already been found, like noise barriers.

46 Noise barriers are civil engineering elements located along roadways and designed to protect
47 inhabitants from noise pollution. These elements, often placed between heavy-traffic roads and
48 residences, also have a beneficial impact on air quality. Indeed, several authors have
49 investigated the efficiency of noise barriers in reducing atmospheric pollutant concentrations
50 behind the barriers using in-field (Baldauf et al., 2008, 2016; Finn et al., 2010; Hagler et al.,
51 2012; Lee et al., 2018; Ning et al., 2010), wind tunnel (Heist et al., 2009) measurements and
52 numerical models (Bowker et al., 2007; Hagler et al., 2011; Schulte et al., 2014). Some authors
53 have studied the effects of barrier heights and distances on pollution reduction (Amini et al.,
54 2018; Gong and Wang, 2018). Other authors have studied the effects of barrier shapes and
55 locations on improving the reduction of atmospheric pollutants (Brechler and Fuka, 2014;

56 Enayati Ahangar et al., 2017; Wang and Wang, 2019). However, although some of these works
57 have been performed by considering different atmospheric stabilities, knowledge is lacking on
58 how the combination of wind conditions and thermal effects can affect pollutant reductions
59 behind barriers. Further work is thus required in this direction.

60 The aim of this work is to study the combined effects of wind and thermal effects on the
61 reduction of pollutant concentrations behind the noise barrier. More specifically, computational
62 fluid dynamics (CFD) simulations are used to assess the evolution of the concentration
63 reduction rate behind noise barriers for several wind speeds and atmospheric stabilities, ranging
64 from very unstable to stable conditions, including all the intermediate conditions (unstable,
65 slightly unstable, neutral and slightly stable). The two key parameters of this study are defined
66 and described in Section 2. The numerical model, including the governing equations, boundary
67 conditions and model validation used in this work, is presented in Section 3. The results of the
68 study are presented in Section 4, after which these results are discussed in Section 5.

69 **2. Description of the study**

70 This paper examines the impact of wind speed and atmospheric stability on the reduction of
71 downwind air pollution induced by the presence of noise barriers. It is therefore necessary to
72 define two recurring parameters: the Richardson number and the concentration reduction rate.

73 The thermal effects can be quantified using the Richardson number noted Ri . The
74 corresponding equation taken from (Woodward, 1998) is given in (1).

$$75 \quad Ri = \frac{gH}{U_H^2} \frac{(T_H - T_w)}{T_{air}} \quad (1)$$

76 where g is the gravitational acceleration, H is the noise barrier height, U_H is the reference
77 velocity (which is the velocity at $z = H$ in this study), T_{air} is the ambient temperature, T_H is

78 the temperature at $z = H$, and T_w is the surface temperature of the heated ground. The difference
79 $T_H - T_w$ will be noted ΔT in the following.

80 The Richardson number is also an indicator of atmospheric stability: $Ri = 0$ corresponds to
81 isothermal (neutral) cases, $Ri < 0$ corresponds to unstable cases, and $Ri > 0$ to stable cases. A
82 better discretization of atmospheric stability, related to Pasquill's stability classes, also exists
83 (Woodward, 1998) and is summarized in Table 1

84

85

Table 1. Atmospheric stability correlated with the Richardson number (Woodward, 1998).

Atmospheric stability	Richardson number
Very unstable	$Ri < -0.86$
Unstable	$-0.86 \leq Ri < -0.37$
Slightly unstable	$-0.37 \leq Ri < -0.10$
Neutral	$-0.10 \leq Ri < 0.053$
Slightly stable	$0.053 \leq Ri < 0.134$
Stable	$0.134 \leq Ri$

86

87 The reduction of the pollution behind the noise barriers compared to an area without these
88 barriers is quantified using an indicator called concentration reduction rate (CRR) given in (2).

$$89 \quad CRR (\%) = \left(1 - \frac{C_{nb}}{C_{ref}}\right) \times 100 \quad (2)$$

90 where C_{nb} is the concentration with a noise barrier and C_{ref} is the reference concentration
91 corresponding to the same case but without noise barriers.

92 The CRR provides information on both the positive and negative impact of noise barriers
93 ($CRR > 0$ means that noise barriers reduce downwind pollution; $CRR < 0$ means that noise
94 barriers increase downwind pollution) and their effectiveness ($CRR = 40\%$ means that the
95 concentration behind noise barriers is reduced by 40% compared to the same case without
96 them).

97 3. Numerical model

98 3.1. Governing equations

99 Simulations were performed using the *buoyantPimpleFoam* solver from OpenFOAM 6.0. This
 100 transient solver is able to resolve Navier-Stokes equations for buoyant and turbulent flows of
 101 compressible fluids including the effects of forced convection (induced by the wind) and natural
 102 convection (induced by heat transfers). The corresponding continuity (3), momentum (4) and
 103 energy (5) equations are given below:

$$104 \quad \frac{\partial \rho}{\partial t} + \nabla \cdot (\rho u) = 0 \quad (3)$$

$$105 \quad \rho \left(\frac{\partial u}{\partial t} + u \cdot \nabla u \right) = -\nabla p + \nabla \cdot \left(2\mu_{eff} D(u) \right) - \nabla \cdot \left(\frac{2}{3} \mu_{eff} (\nabla \cdot u) \right) + \rho u \quad (4)$$

$$106 \quad \frac{\partial \rho e}{\partial t} + \nabla \cdot (\rho u e) + \frac{\partial \rho K}{\partial t} + \nabla \cdot (\rho u K) + \nabla \cdot (u p) = \nabla \cdot (\alpha_{eff} \nabla e) + \rho g \cdot u \quad (5)$$

$$107 \quad D(u) = \frac{1}{2} [\nabla u + (\nabla u)^T] \quad (6)$$

$$108 \quad K \equiv |u|^2/2 \quad (7)$$

109 where u is the velocity, p the pressure, ρ the density, e the thermal energy, $D(u)$ the rate of
 110 strain tensor given in (6), K the kinetic energy given in (7), g the gravitational acceleration,
 111 μ_{eff} the effective viscosity defined as the sum of molecular and turbulent viscosity and α_{eff}
 112 the effective thermal diffusivity defined as the sum of laminar and turbulent thermal
 113 diffusivities.

114 No chemical reactions are considered in this study. Thus, the equation governing passive scalar
 115 transport (8) has been added to the solver. This advection-diffusion equation is given below:

116

117
$$\frac{\partial C}{\partial t} + \nabla \cdot (uC) - \nabla \cdot \left[\left(D_m + \frac{\nu_t}{Sc_t} \right) \nabla C \right] = E \quad (8)$$

118 where C is the pollutant concentration, D_m the molecular diffusion coefficient, ν_t the turbulent
 119 diffusivity, Sc_t the turbulent Schmidt number and E the source term of the pollutants
 120 (emissions).

121 A Reynolds-averaged Navier-Stokes (RANS) methodology was used to resolve the equations.
 122 When using this methodology, a new term called Reynolds stress tensor appear and it is
 123 necessary to choose a turbulence model to resolve it. The RNG k- ϵ turbulence model proposed
 124 by Yakhot et al. (1992) has been selected because it gives significant improvements compared
 125 to the standard turbulence model for recirculatory flows (Papageorgakis and Assanis, 1999),
 126 whereas anisotropic models such as the Reynolds Stress Model (RSM) may not improve the
 127 results (Koutsourakis et al., 2012) for a higher calculation cost and more calculation
 128 instabilities.

129 Each simulation was performed using second order schemes for all the gradient, divergent and
 130 Laplacian terms. The streamwise velocity U and the pollutant concentration C were monitored
 131 for several locations behind the downwind noise barrier and the results were checked to ensure
 132 that each simulation has converged. At the end of the simulations, all the residuals were under
 133 10^{-5} .

134 3.2. Computational domain and boundary conditions

135 This study focuses on the concentration reduction rates induced by the presence of noise
 136 barriers. Thus, to quantify this reduction, two distinct cases have to be considered in terms of
 137 computational domain: a case with noise barriers and a case without them. Fig. 1 shows a sketch
 138 of the computational domain and the boundary conditions used for the case with noise barriers.
 139 The second case is strictly the same but without the noise barriers.

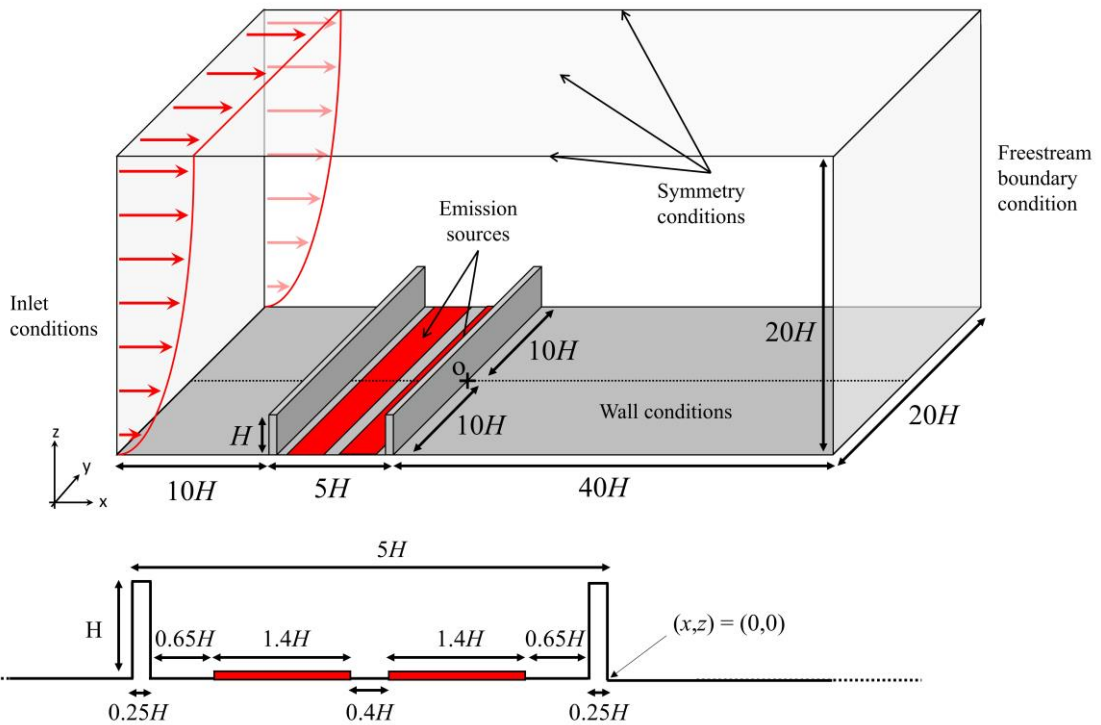


Fig.1. Sketch of the computational domain with $H = 0.5$ m.

140

141

142

143 The recommendations given by Franke et al. (2007) were followed concerning the boundary
 144 conditions and domain size. The inlet boundary is localized $10H$ before the upwind noise barrier
 145 where velocity, turbulence and temperature profiles are specified using a perpendicular wind
 146 direction, unless otherwise stated. The outlet boundary is placed $40H$ behind the downwind
 147 noise barrier with a freestream condition to allow the flow to fully develop. Symmetry
 148 conditions are applied for the upper and lateral limits, with the top of the calculation domain
 149 placed $20H$ from the ground and the lateral limits located $20H$ from each other. No-slip
 150 conditions are applied to any other boundaries including the ground and the two noise barriers,
 151 where the temperature can be specified to simulate stable and unstable cases. Finally, traffic
 152 exhausts are modeled by two volumetric sources along the y -direction, with a width of $1.4H$
 153 each, and over one mesh height (0.25 m) where an emission source term is added in the pollutant
 154 transport equation. A mass flow rate of 100 g/s is used for all the simulations performed. Further
 155 information can be found in Table 2.

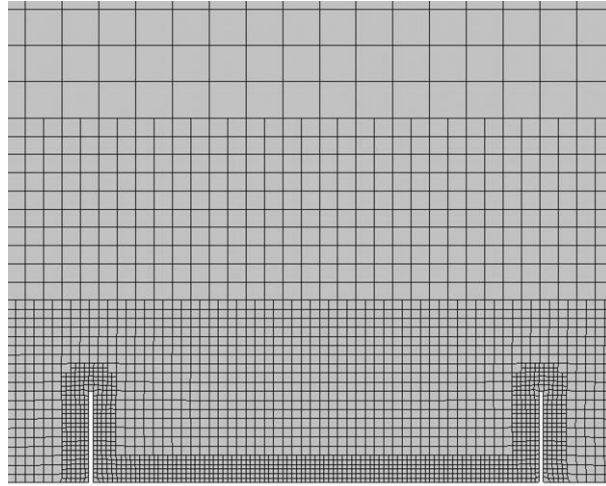
156

Table 2. Summary of the boundary conditions.

	Velocity and turbulence profiles are calculated according to Richards and Norris (2011):
	$U = \frac{u_*}{\kappa} \ln\left(\frac{z}{z_0}\right) \quad (9) \quad k = \frac{u_*^2}{\sqrt{C_\mu}} \quad (10) \quad \varepsilon = \frac{u_*^3}{\kappa z} \quad (11)$
Inlet	with U the wind velocity, k the turbulent kinetic energy (TKE), ε the dissipation of TKE, u_* the friction velocity, κ the von Kármán constant taken to 0.41, z the altitude, z_0 the roughness height taken as 0.5 m, and C_μ a CFD constant taken as 0.085. Fixed temperature: $T_{air} = 293$ K.
Outlet	Freestream outlet.
Top	Symmetry plane.
Lateral surfaces	Symmetry plane.
Ground and noise barriers surfaces	No-slip condition ($U = 0$ m/s). Fixed temperature (T_w) depending on the case studied.
Emission	Surface source with emission rate $q_m = 100$ g/s.

157

158 Mesh sensitivity tests were carried out to ensure that the results are fully independent of mesh
159 size. Successive simulations were performed with different mesh sizes and the Grid
160 Convergence Index (*GCI*) methodology (Roache, 1994) was used to assess the mesh-related
161 errors on both the flow field and the concentration field. Mean *GCI*s of 2% and 1% were
162 obtained for flow and concentration fields, respectively, when comparing the results from mesh
163 sizes of 0.5 m and 0.25 m. Thus, a mesh size of 0.5 m was considered sufficient to avoid
164 excessive calculation costs and was used for the study. This mesh size corresponds to the
165 meshes localized between an altitude of $z = 0$ and $z = 2H$. However, greater refinement was
166 applied near the noise barrier walls and the road because of the strong gradients that can occur
167 in these areas. This mesh size resulted in a total of 2.6 million meshes and an illustration of the
168 meshes selected is provided in Figure 2. The meshing was done using the unstructured grid
169 generator *snappyHexMesh* available with OpenFOAM.



170

171

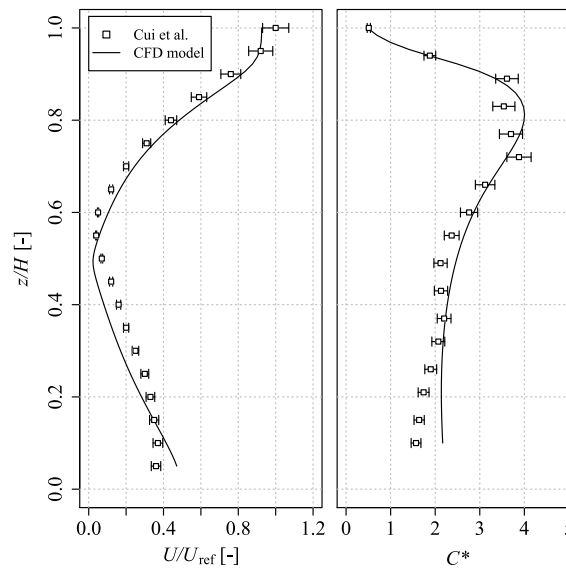
Fig.2. Grid selected for computation.

172 3.3. Model validation

173 The numerical model was compared against the experimental data proposed by Cui et al. (2016)
174 because they provided results on both velocity and the concentration field for a complex 3D
175 situation. Indeed, the experiment setup consists of two buildings with the downwind building
176 being higher than the upwind building. A gas is released at the top of the upwind building and
177 the ground between the two buildings is heated to simulate several atmospheric stabilities and
178 heat exchanges. The downwind building is opened and closed by two windows to simulate
179 indoor/outdoor pollutant exchanges.

180 Fig. 3 shows the comparison between the experimental data and the numerical model used in
181 this study for a stable case where $Ri = 1.22$ ($U_{free\ stream} = 0.7$ m/s and $\Delta T = 135$ °C) and for a
182 vertical profile localized between the two buildings. These results are presented in a
183 dimensionless form that can be found in the paper of Cui et al. (2016). The results show good
184 agreement between the numerical model and the experimental data on both velocity and
185 concentration profiles, with a mean difference of 6% between the experimental and numerical
186 concentration profiles. The numerical model is therefore capable of accurately reproducing

187 velocity and concentration profiles in a 3D case with a high thermal gradient. According to
 188 these results, the numerical model was considered validated for the purpose of this study.



189
 190 Fig.3. Vertical distribution of dimensionless velocity and concentration for $Ri = 1.22$ given by Cui *et al.* for the wind tunnel
 191 measurements (Cui *et al.*, 2016), and comparison with the CFD model with $Sc_t = 0.25$.

192 4. Results

193 Several simulations were performed to study the combined effects of wind speed and thermal
 194 effects on the concentration reduction rate behind the barriers. All the simulations performed
 195 with their specific conditions (U_H and ΔT) and their corresponding Richardson numbers are
 196 given in Table 3. Each of these conditions was simulated twice to obtain results with and
 197 without noise barriers to calculate the concentration reduction rates. A total of 64 simulations
 198 were carried out including:

- 199 - 24 simulations for the neutral case (6 simulations for each of the three turbulent Schmidt
- 200 numbers considered to assess their impact on the concentration reduction rates and 6
- 201 supplementary simulations for a non-perpendicular case);
- 202 - 20 simulations for the stable cases;
- 203 - 20 simulations for the unstable cases.

204 All the results were extracted at the center of the computational domain along $y/H = 0$ with
 205 $x/H = 0$ corresponding to the end of the downwind noise barrier wall.

206 Table 3. Summary of the simulations performed with wind velocity and thermal conditions ($\Delta T = T_H - T_w$) and
 207 their corresponding Richardson numbers.,

U_H [m/s]	1.18	1.96	3.15	5.51	7.87
Ri [-]					
0	$\Delta T = 0$ K		$\Delta T = 0$ K	$\Delta T = 0$ K	
0.06				$\Delta T = 10$ K	
0.17			$\Delta T = 10$ K	$\Delta T = 30$ K	$\Delta T = 62$ K
0.33		$\Delta T = 7.5$ K	$\Delta T = 19.5$ K		
0.50		$\Delta T = 11.5$ K	$\Delta T = 29.5$ K		
1.20	$\Delta T = 10$ K	$\Delta T = 27.5$ K			
-0.06				$\Delta T = -10$ K	
-0.17			$\Delta T = -10$ K	$\Delta T = -30$ K	$\Delta T = -62$ K
-0.50		$\Delta T = -11.5$ K	$\Delta T = -29.5$ K		
-0.75		$\Delta T = -17.5$ K	$\Delta T = -44.5$ K		
-1.20	$\Delta T = -10$ K		$\Delta T = -71$ K		

208

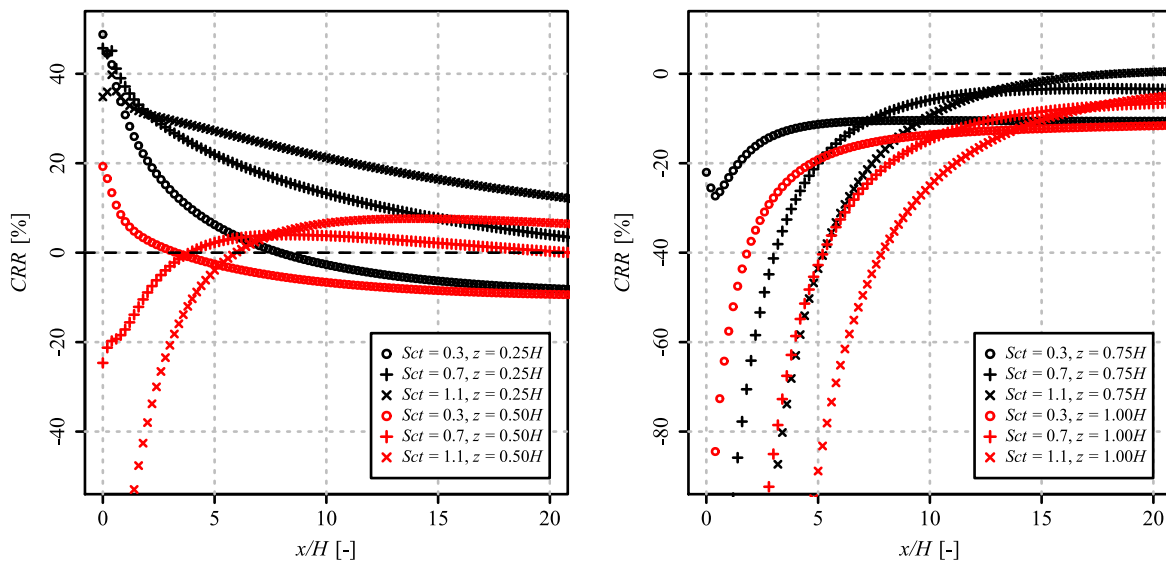
209 4.1. Study without thermal effects

210 4.1.1. Turbulent Schmidt number sensitivity

211 The turbulent Schmidt number (Sc_t) is a dimensionless number found in air pollution CFD to
 212 consider the effect of turbulent diffusivity. However, this number is widely spread between 0.2
 213 and 1.3, depending on the situation studied, and can significantly change the results in terms of
 214 concentration (Tominaga and Stathopoulos, 2007). To assess the effect of this parameter on
 215 noise barrier studies, three Sc_t were considered: 0.3, 0.7 and 1.1.

216 The evolutions of the CRR behind the barriers for the three Sc_t considered and for four altitudes
 217 ($z = 0.25H, 0.50H, 0.75H$ and $1.00H$) are presented in Fig. 4 as a function of the dimensionless
 218 distance from the downwind noise barrier x/H . The results show considerable variability for the
 219 concentration reduction rate as a function of the turbulent Schmidt number and no general trend

220 can be observed. Indeed, while for $Sc_t = 1.1$ and $z = 0.25H$ the CRR is globally higher than for
 221 other turbulent Schmidt numbers, for the three other altitudes the CRR is not globally higher.
 222 Additionally, while the CRR is globally lower with $Sc_t = 0.3$ and $z = 0.25H$, this observation is
 223 no longer true for the other altitudes. Moreover, the turbulent Schmidt number has also an
 224 impact on the distance after the barriers were there is a positive impact of the noise barriers
 225 ($CRR > 0$), this distance being higher for higher Sc_t .



226
 227 Fig.4. Evolution of the concentration reduction rate behind the downwind wall as a function of Sc_t and for several altitudes
 228 with the same wind profile ($U_H = 1.18$ m/s).

229
 230 According to these results, it is important to state that the turbulent Schmidt number is also a
 231 very sensitive parameter when studying the impacts of noise barriers and its choice should be
 232 considered carefully, especially when performing quantitative studies. For the rest of this paper,
 233 and since no information or studies to determine the best turbulent Schmidt number for noise
 234 barrier studies are available an intermediate turbulent Schmidt number of 0.7 is used and the
 235 results are presented qualitatively rather than quantitatively.

236

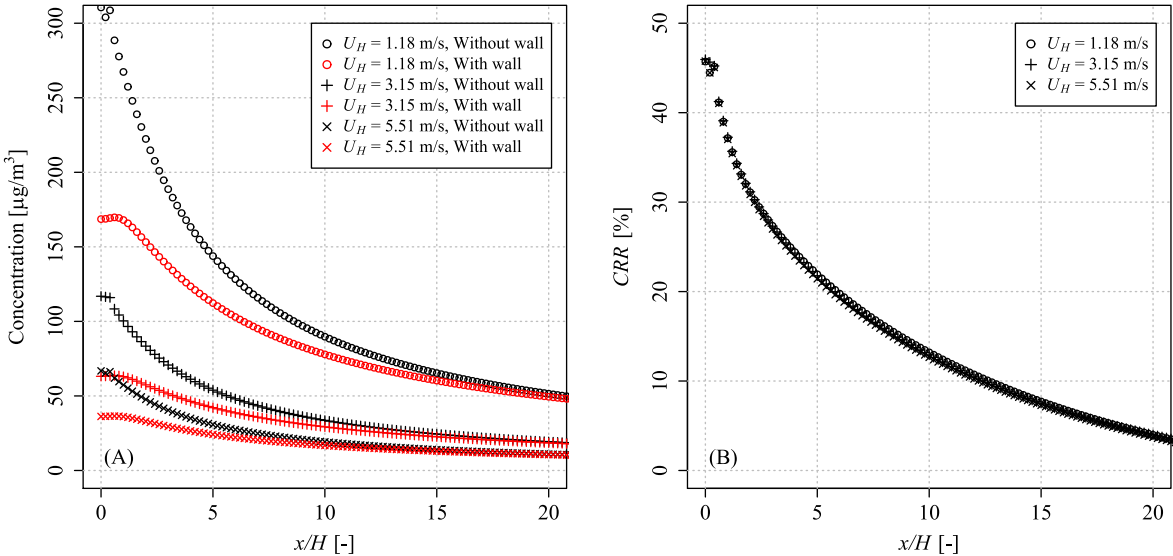
237

238 *4.1.2. Impact of wind speed and wind direction on the CRR in neutral atmosphere*

239 The impact of wind speed and wind direction on the concentration reduction rate was first
240 studied in neutral atmosphere, thus, considering only forced convection (i.e. convection due to
241 the wind).

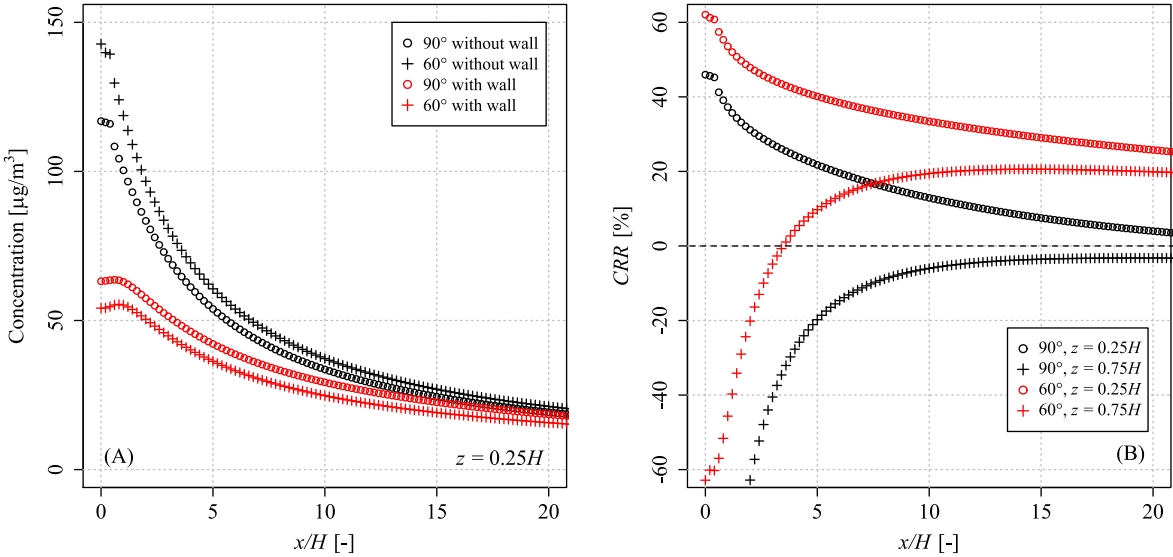
242 Fig. 5 shows the evolution of the pollutant concentrations behind the barriers for the cases with
243 and without barriers (A) and the corresponding concentration reduction rates (B) as a function
244 of the wind speed at $z = 0.25H$. According to Fig. 5 (A), regardless of the wind speed and for
245 $z = 0.25H$, pollutant concentrations were generally higher without the noise barrier than with it.
246 Additionally, concentrations changed inversely with wind speed, leading to lower
247 concentrations for higher wind speeds. The concentrations were thus different as a function of
248 this parameter. However, as depicted in Fig. 5 (B), the *CRR* is the same whatever the wind
249 speed considered and this is also true for the other altitudes considered ($z = 0.5H$, $0.75H$ and
250 $1.00H$). This result is linked to the fact that, for a given wind direction and without thermal
251 stratification, the concentration was inversely proportional to the wind velocity (Schatzmann
252 and Leitl, 2011). Thus, since the concentration evolved in the same way with wind speed both
253 with and without noise barriers, the *CRR* remained unchanged for a given wind direction under
254 neutral conditions.

255 The effects of the wind direction under neutral conditions were also investigated and the results
256 are presented in Fig. 6 for a perpendicular wind (90°) and a wind oriented at 60° . Fig 6 (A)
257 shows that for the 60° case, the concentrations are lower with the noise barriers and higher
258 without the noise barriers compared to the perpendicular case. This inevitably leads to a lower
259 *CRR* for the perpendicular case, as shown in Fig. 6 (B) for $z = 0.25H$ and $z = 0.75H$. The same
260 result was obtained for $z = 0.50H$ and $z = 1.00H$. Therefore, the *CRR* are higher for oblique
261 wind directions.



262
263 Fig.5. Evolution of the concentrations with and without noise barriers (A) and the concentration reduction rates (B) as a
264 function of wind speed for a perpendicular wind direction at $z = 0.25H$.

265
266



267
268 Fig.6. Evolution of the concentrations with and without noise barriers (A) and the concentration reduction rates (B) as a
269 function of the wind direction and for a given wind speed ($U_H = 3.15$ m/s).

270
271

272 According to the previous results, when studying the CRR behind noise barriers for neutral
273 cases, it is necessary to study only one wind speed for each wind direction. Moreover, if the
274 minimal CRR is assessed, the study can be reduced to only one direction. Indeed, the
275 perpendicular direction leads to the lowest CRR while the non-perpendicular directions lead to
276 higher CRR.

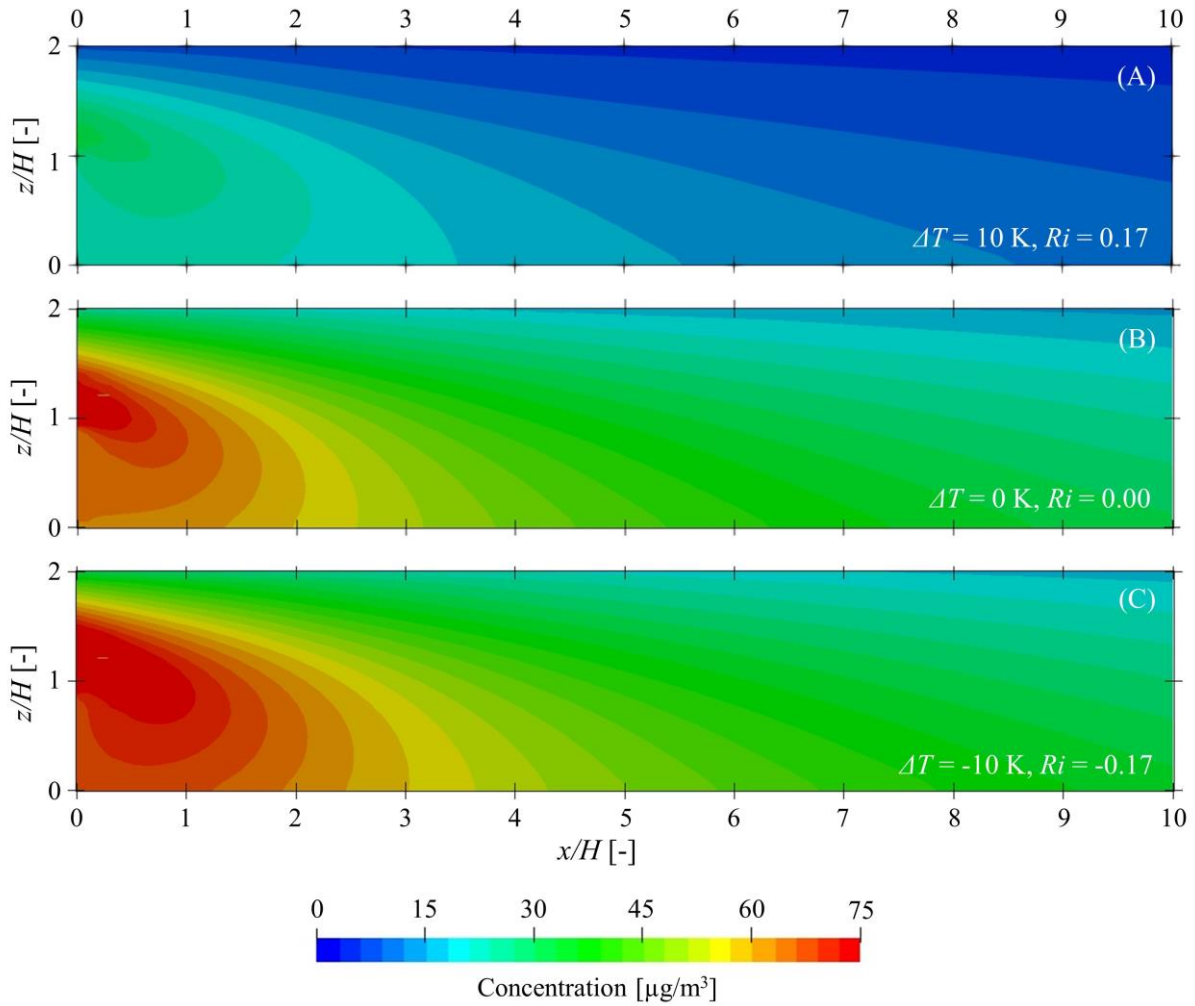
277

278 4.2. Study with thermal effects

279 4.2.1. Evolution of the CRR as a function of the atmospheric stability

280 The concentration reduction rate was then studied considering mixed convection: forced
281 convection induced by wind speed and natural convection induced by thermal stratifications.
282 The CRR was therefore studied as a function of the Richardson number which includes wind
283 speed (U_H) and thermal variations (ΔT).

284 The first results are presented in Fig. 7 for three different Richardson numbers: (A) $Ri = -0.17$
285 corresponding to a stable atmosphere; (B) $Ri = 0$ corresponding to a neutral atmosphere; and
286 (C) $Ri = -0.17$ corresponding to a slightly unstable atmosphere, for the same wind conditions
287 (perpendicular wind with $U_H = 3.15$ m/s). Thus, ΔT is the only variable here. For the three cases
288 considered, the concentration is highest directly behind the barriers ($x = 0$ m), just above them
289 ($h = 5$ m) and generally decreases as the distance from the barrier increases or the height
290 decreases. However, the concentrations are different depending on the case. Indeed, the
291 concentrations are lowest for the stable case (A) and highest for the slightly unstable case (C).
292 The neutral case (B) leads to intermediate results but closer to the unstable one. For a given
293 wind speed and direction, thermal effects therefore have a high impact on the concentration
294 behind the barriers and seem to have a greater impact for $\Delta T > 0$ than for $\Delta T < 0$.



295

296 Fig.7. Evolution of the concentration behind the downwind barrier as a function of the temperature variation in the same

297

wind conditions (perpendicular wind, $U_H = 3.15$ m/s).

298

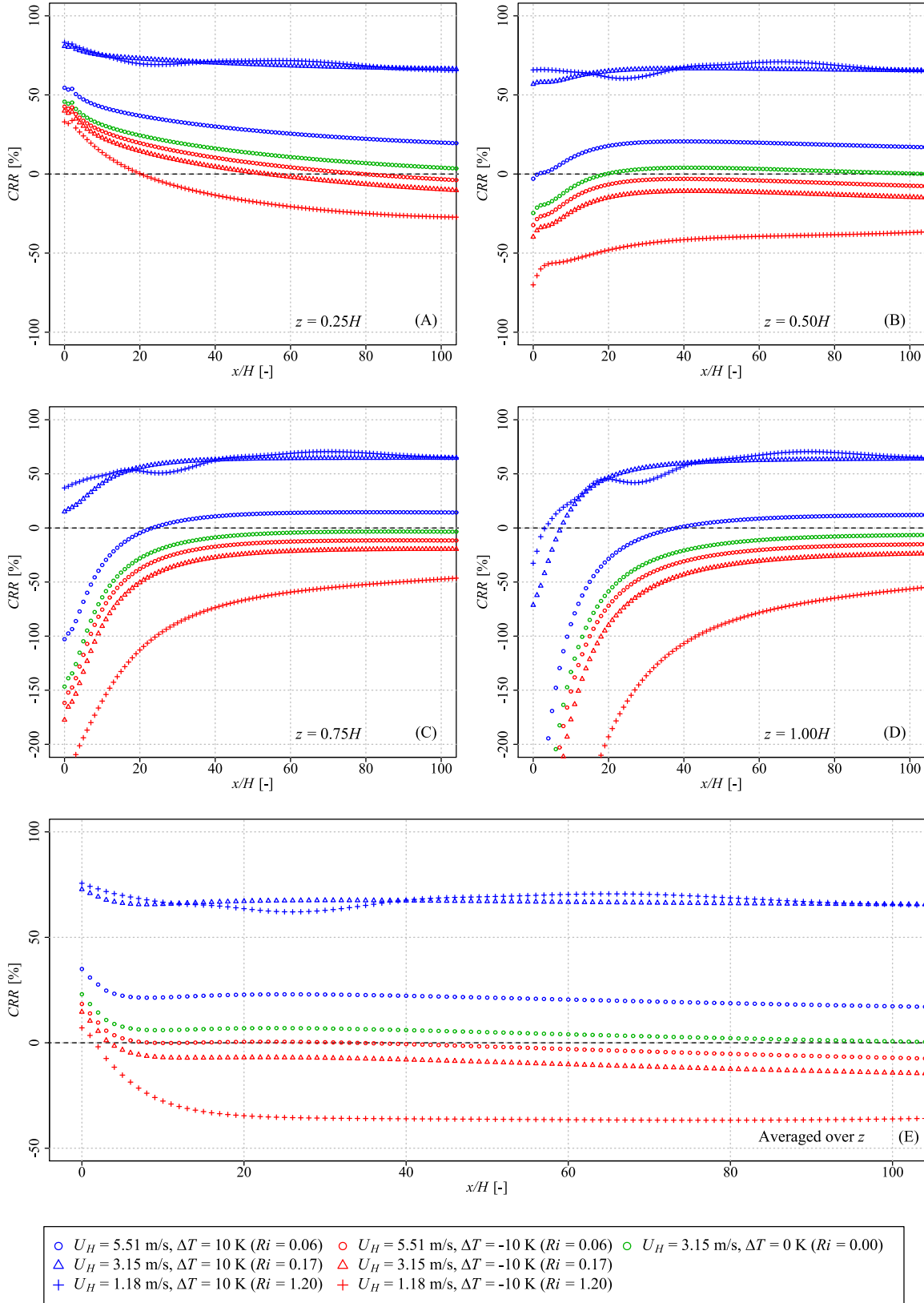
299 The evolution of the *CRR* as a function of the distance from the downwind barrier was studied300 for several atmospheric stabilities by changing both the wind speed (U_H) and the thermal301 variation (ΔT). The results for $Ri = -1.20, -0.17, -0.06, 0.00, 0.17, 0.06$ and 1.20 are given in302 Fig. 8 for $z = 0.25H$ (A), $0.50H$ (B), $0.75H$ (C) and $1.00H$ (D). Further results are presented in303 Fig. 8 (E) and correspond to the *CRR* averaged over z for z ranging from 0 to 5 m giving global

304 information along the height of the noise barriers.

305 As can be seen in Fig. 8, the evolution of the *CRR* follow the same trends. Indeed, for all the
306 altitudes considered and also for the *CRR* averaged over $z = H$, the results for the neutral case
307 are bounded by the results for the stable cases and the unstable cases: the unstable cases lead to
308 lower *CRRs* compared to the neutral case, with the lowest *CRR* being obtained for the highest
309 instability level ($Ri = -1.20$). On the contrary, the stable cases lead to higher *CRRs* with the
310 highest *CRR* being obtained for the highest stability level ($Ri = 1.20$). However, the evolution
311 of the *CRR* according to the level of stability or instability is not equivalent between the two
312 cases. Indeed, whereas the results are different for the three unstable cases presented in Fig. 8,
313 the *CRR* for the two highest stable cases ($Ri = 0.17$ and $Ri = 1.20$) are very similar. Furthermore,
314 the *CRR* changes more quickly as a function of the Richardson number for the stable cases than
315 for the unstable cases, which is consistent with the previous results discussed in relation with
316 Fig. 7. Thus, atmospheric stability has an impact on the *CRR*, leading to higher *CRRs* for stable
317 cases ($Ri > 0$), quickly reaching maximum values, while lower *CRRs* are obtained for unstable
318 cases ($Ri < 0$) and no maximum values were reached for the Richardson numbers considered in
319 this study.

320 Fig. 8 also shows that the *CRR* not only depends on the distance from the barriers but also on
321 their height. For a given atmospheric stability, the *CRR* decreases with height and can reach
322 negative values corresponding to an increase in pollutant concentration due to the barriers.
323 These observations are related to the heights at which the plumes spread in both configurations,
324 with and without the barriers. Indeed, without the noise barriers the plume spreads along the
325 ground, leading to lower concentrations at $z = H$, while with the noise barriers the plume spreads
326 from the top of the barriers and the concentrations are generally lower at ground level compared
327 to the case without barriers.

328



329

330

331

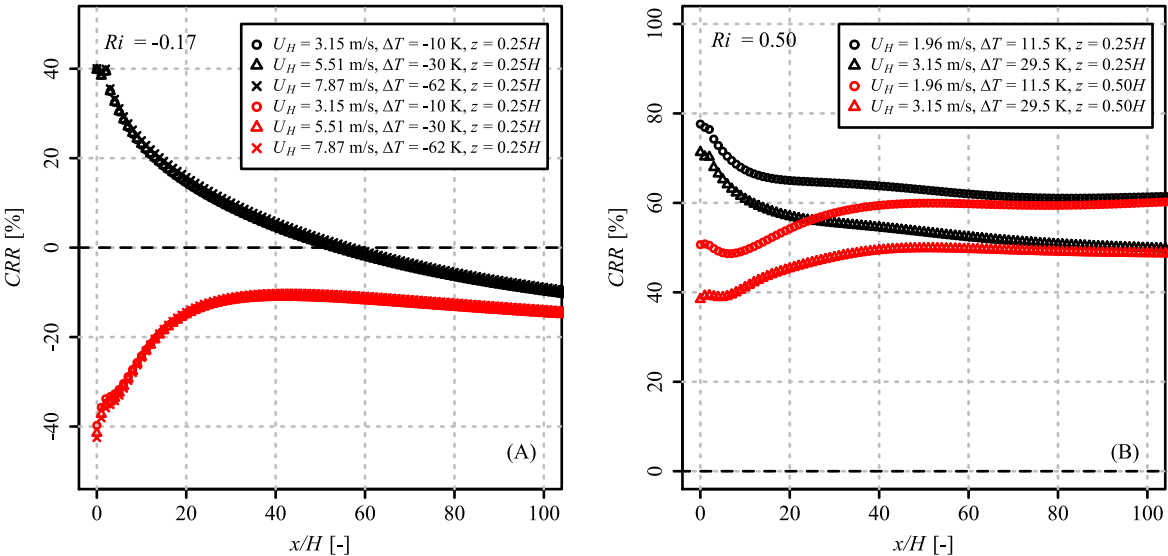
Fig.8. Evolution of the concentration reduction rates for 4 given altitudes (A—D) and averaged over the noise barrier height (E) as a function of the distance from the downwind barrier and for several Richardson numbers.

332 4.2.2. Conservation of the *CRR* with the Richardson number

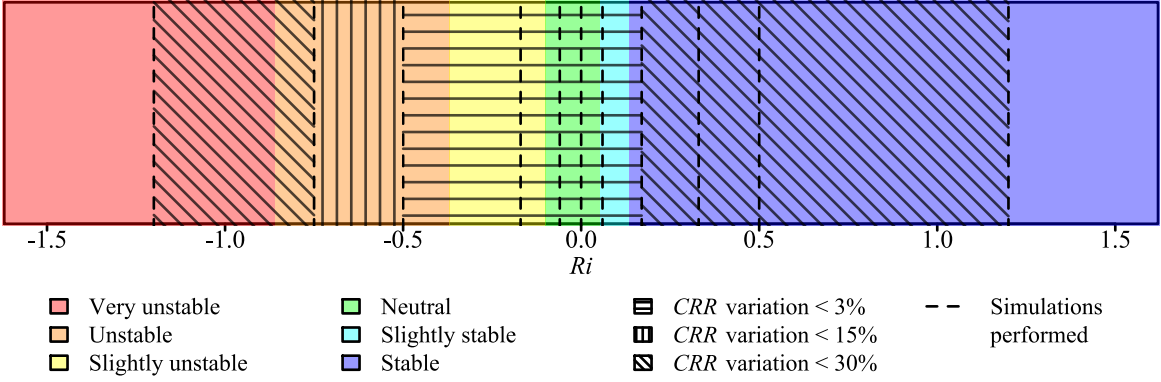
333 It has been shown previously that the concentration reduction rate for a given wind direction is
334 constant when considering only forced convection (neutral atmosphere) due to an inversely
335 proportional link between the pollutant concentrations and the wind speed. However, this link
336 is no longer valid when considering both forced and natural convection. The question was then
337 to assess if the *CRR* is still constant for stable and unstable cases. To answer this question,
338 several simulations were performed for numerous Richardson numbers but with distinct couples
339 of wind speed and thermal variations. The Richardson numbers considered were $Ri = -1.20$,
340 -0.75 , -0.50 , -0.17 , -0.06 , 0.00 , 0.06 , 0.17 , 0.33 , 0.50 and 1.50 .

341 Fig. 9 (A) shows the evolution of the *CRR* for three couples of U_H and ΔT giving $Ri = -0.17$
342 (slightly unstable atmosphere) while Fig. 9 (B) shows the evolution of the *CRR* for two couples
343 giving $Ri = 0.50$ (stable atmosphere). According to Fig. 9 (A), the *CRR* can be constant for a
344 given Ri . Indeed, with $Ri = -0.17$, while the pollutant concentrations are not the same for the
345 three couples of U_H and ΔT considered, the *CRR* is quasi-constant ($\pm 3\%$). However, this
346 observation is not true for all the Richardson numbers according to Fig. 9 (B), which shows that
347 for $Ri = 0.50$ the *CRRs* are significantly different for the two couples of U_H and ΔT considered.
348 Thus, the *CRR* can be constant for a given Ri but this is not generalizable.

349 The Richardson numbers for which the *CRR* can be considered constant were assessed and the
350 results are presented in Fig. 10. The results show that, for a Ri ranging from -0.50 to 0.17 , the
351 variation over the *CRR* is less than 3% and the *CRR* can be considered as constant for a given
352 Ri . For Richardson numbers outside this range, the variation over the *CRR* for a given Ri can
353 reach 15% for a Ri ranging from -0.75 to -0.5 and 30% for a Ri ranging from -0.75 to -1.20 and
354 from 0.17 to 1.20 . According to these results, for a given Ri ranging from -0.50 to 0.17 , a unique
355 couple of U_H and ΔT must be considered when assessing the concentration reduction rates
356 behind noise barriers in non-neutral cases.



357
 358 Fig.9. Evolution of the concentration reduction rate for $Ri = -0.17$ (A) and $Ri = 0.50$ (B) as a function of wind speed (U_H) and
 359 thermal variation (ΔT) at $z = 0.25H$ and $z = 0.50H$.
 360



361
 362 Fig.10. Conservation of the concentration reduction rate with the Richardson number.

363 **5. Discussion**

364 This study provides better understanding of how noise barriers can reduce air pollution and how
 365 this reduction can vary with wind conditions and atmospheric stability. Additional work can be
 366 done to further improve this understanding and is discussed below, as is the relevance of these
 367 results.

368 It was shown that for a given Ri ranging from -0.50 to 0.17, variations over the CRR are
369 negligible. Moreover, the evolution of the CRR as a function of distance from the downwind
370 barrier seemed to follow the same trends, as the curves appear the same. Thus, it may be
371 possible to find relationships between the CRR and the Richardson number in the range -0.50
372 to 0.17. If such relationships can be found, it will allow estimating all the $CRRs$ in this Ri range
373 by performing only one simulation, or with only one in-field measurement.

374 This study considered only one noise barrier configuration, with two walls of the same height
375 placed on either side of a heavy-traffic road. Further studies could be performed to verify if the
376 results obtained for this configuration are generalizable, for example for noise barriers with
377 only one upwind or downwind wall and also with a combination of solid and vegetative barriers.
378 Finally, according to the results of this study, further studies can be simplified. Indeed, for
379 future studies in neutral atmosphere (without thermal variations), they could be reduced to only
380 wind direction and noise barrier configuration studies when assessing the evolution of the CRR .
381 For studies including mixed convection (with thermal variations), for a Ri ranging from -0.50
382 to 0.17, only one couple of wind speed and thermal variation is needed to assess the evolution
383 of the CRR .

384 **6. Conclusion**

385 The effects of wind speed and atmospheric stability on the concentration reduction rate (CRR)
386 of air pollutants induced by noise barriers were studied with a validated CFD model. This study
387 considered both numerous wind conditions (wind speed and direction) and thermal variations,
388 leading to different atmospheric stabilities ranging from very unstable cases to stable cases.
389 Several CFD simulations were carried out and the main conclusions are as follows:

- 390 (a) When no thermal variations are considered, i.e. for a neutral atmosphere, the evolution
391 of the *CRR* depends only on the wind direction: wind speed changes the pollutant
392 concentrations behind the barriers but this parameter does not change the *CRR*.
- 393 (b) A non-perpendicular wind direction leads to higher pollutant concentrations without
394 noise barriers and lower concentrations with the barriers compared to perpendicular
395 cases. The *CRRs* are therefore minimal for a perpendicular wind.
- 396 (c) The *CRR* decreases with height due to the different locations of the plume for the two
397 cases with and without noise barriers. The global *CRR* decreases with distance from the
398 downwind barrier.
- 399 (d) The *CRR* obtained with forced convection (neutral atmosphere) is bounded by the *CRR*
400 obtained with mixed convection (stable and unstable atmospheres): higher *CRRs* are
401 obtained in stable conditions ($Ri > 0$) while lower *CRRs* are obtained in unstable
402 conditions ($Ri < 0$).
- 403 (e) For a given Richardson number ranging from -0.50 to 0.17, the *CRR* is constant with a
404 variation of less than 3%. For numbers outside this range the variation increases to 15%
405 for a Ri ranging from -0.75 to -0.5 and 30% for a Ri ranging from -1.20 to -0.75 and
406 from 0.17 to 1.20.

407 Finally, these results give insights to researchers and civil engineers to better understand
408 variations of air pollutant concentrations behind noise barriers, for example for carrying out
409 further assessment studies on the impact of noise barriers on the reduction of air pollution, and
410 for in-field monitoring campaigns.

411 **Acknowledgments**

412 We would like to thank the ANRT (Association Nationale de la Recherche et de la Technologie)
413 for their support.

414 **References**

- 415 Amini, S., Ahangar, F.E., Heist, D.K., Perry, S.G., Venkatram, A., 2018. Modeling dispersion
 416 of emissions from depressed roadways. *Atmospheric Environment* 186, 189–197.
 417 <https://doi.org/10.1016/j.atmosenv.2018.04.058>
- 418 Anderson, J.O., Thundiyil, J.G., Stolbach, A., 2012. Clearing the Air: A Review of the Effects
 419 of Particulate Matter Air Pollution on Human Health. *J. Med. Toxicol.* 8, 166–175.
 420 <https://doi.org/10.1007/s13181-011-0203-1>
- 421 Baldauf, R., Thoma, E., Khlystov, A., Isakov, V., Bowker, G., Long, T., Snow, R., 2008.
 422 Impacts of noise barriers on near-road air quality. *Atmospheric Environment* 6.
 423 <https://doi.org/10.1016/j.atmosenv.2008.05.051>
- 424 Baldauf, R.W., Isakov, V., Deshmukh, P., Venkatram, A., Yang, B., Zhang, K.M., 2016.
 425 Influence of solid noise barriers on near-road and on-road air quality. *Atmospheric*
 426 *Environment* 129, 265–276. <https://doi.org/10.1016/j.atmosenv.2016.01.025>
- 427 Bowker, G.E., Baldauf, R., Isakov, V., Khlystov, A., Petersen, W., 2007. The effects of roadside
 428 structures on the transport and dispersion of ultrafine particles from highways.
 429 *Atmospheric Environment* 41, 8128–8139.
 430 <https://doi.org/10.1016/j.atmosenv.2007.06.064>
- 431 Brechler, J., Fuka, V., 2014. Impact of Noise Barriers on Air-Pollution Dispersion. *NS* 06, 377–
 432 386. <https://doi.org/10.4236/ns.2014.66038>
- 433 Chen, H., Kwong, J.C., Copes, R., Tu, K., Villeneuve, P.J., van Donkelaar, A., Hystad, P.,
 434 Martin, R.V., Murray, B.J., Jessiman, B., Wilton, A.S., Kopp, A., Burnett, R.T., 2017.
 435 Living near major roads and the incidence of dementia, Parkinson’s disease, and
 436 multiple sclerosis: a population-based cohort study. *The Lancet* 389, 718–726.
 437 [https://doi.org/10.1016/S0140-6736\(16\)32399-6](https://doi.org/10.1016/S0140-6736(16)32399-6)
- 438 Cui, P.-Y., Li, Z., Tao, W.-Q., 2016. Buoyancy flows and pollutant dispersion through different
 439 scale urban areas: CFD simulations and wind-tunnel measurements. *Building and*
 440 *Environment* 104, 76–91. <https://doi.org/10.1016/j.buildenv.2016.04.028>
- 441 Enayati Ahangar, F., Heist, D., Perry, S., Venkatram, A., 2017. Reduction of air pollution levels
 442 downwind of a road with an upwind noise barrier. *Atmospheric Environment* 155, 1–
 443 10. <https://doi.org/10.1016/j.atmosenv.2017.02.001>
- 444 European Commission, 2013. Proposal for a Directive of the European Parliament and of the
 445 Council on the reduction of national emissions of certain atmospheric pollutants and
 446 amending Directive 2003/35/EC. European Commission (EC), Brussels, Belgium.
- 447 Finkelstein, M.M., Jerrett, M., Sears, M.R., 2004. Traffic Air Pollution and Mortality Rate
 448 Advancement Periods. *American Journal of Epidemiology* 160, 173–177.
 449 <https://doi.org/10.1093/aje/kwh181>
- 450 Finn, D., Clawson, K.L., Carter, R.G., Rich, J.D., Eckman, R.M., Perry, S.G., Isakov, V., Heist,
 451 D.K., 2010. Tracer studies to characterize the effects of roadside noise barriers on near-
 452 road pollutant dispersion under varying atmospheric stability conditions. *Atmospheric*
 453 *Environment* 11. <https://doi.org/10.1016/j.atmosenv.2009.10.012>
- 454 Franke, J., Hellsten, A., Schlünzen, H., Carissimo, B., 2007. Best practice guideline for the
 455 CFD simulation of flows in the urban environment. *COST Action* 732.
- 456 Gong, L., Wang, X., 2018. Numerical Study of Noise Barriers’ Side Edge Effects on Pollutant
 457 Dispersion near Roadside under Various Thermal Stability Conditions. *Fluids* 3, 105.
 458 <https://doi.org/10.3390/fluids3040105>
- 459 Hagler, G.S.W., Lin, M.-Y., Khlystov, A., Baldauf, R.W., Isakov, V., Faircloth, J., Jackson,
 460 L.E., 2012. Field investigation of roadside vegetative and structural barrier impact on
 461 near-road ultrafine particle concentrations under a variety of wind conditions. *Science*
 462 *of The Total Environment* 419, 7–15. <https://doi.org/10.1016/j.scitotenv.2011.12.002>

- 463 Hagler, G.S.W., Tang, W., Freeman, M.J., Heist, D.K., Perry, S.G., Vette, A.F., 2011. Model
464 evaluation of roadside barrier impact on near-road air pollution. *Atmospheric*
465 *Environment* 45, 2522–2530. <https://doi.org/10.1016/j.atmosenv.2011.02.030>
- 466 Heist, D.K., Perry, S.G., Brixey, L., 2009. A wind tunnel study of the effect of roadway
467 configurations on the dispersion of traffic-related pollution. *Atmospheric Environment*
468 43(32). <https://doi.org/10.1016/j.atmosenv.2009.06.034>
- 469 Kagawa, J., 1985. Evaluation of biological significance of nitrogen oxides exposure. *Tokai J.*
470 *Exp. Clin. Med.* 10, 348–353.
- 471 Kim, K.-H., Kabir, E., Kabir, S., 2015. A review on the human health impact of airborne
472 particulate matter. *Environment International* 74, 136–143.
473 <https://doi.org/10.1016/j.envint.2014.10.005>
- 474 Koutsourakis, N., Bartzis, J.G., Markatos, N.C., 2012. Evaluation of Reynolds stress, $k-\epsilon$ and
475 RNG $k-\epsilon$ turbulence models in street canyon flows using various experimental datasets.
476 *Environmental Fluid Mechanics* 12, 379–403. [https://doi.org/10.1007/s10652-012-](https://doi.org/10.1007/s10652-012-9240-9)
477 9240-9
- 478 Lee, E.S., Ranasinghe, D.R., Ahangar, F.E., Amini, S., Mara, S., Choi, W., Paulson, S., Zhu,
479 Y., 2018. Field evaluation of vegetation and noise barriers for mitigation of near-
480 freeway air pollution under variable wind conditions. *Atmospheric Environment* 175,
481 92–99. <https://doi.org/10.1016/j.atmosenv.2017.11.060>
- 482 Ning, Z., Hudda, N., Daher, N., Kam, W., Herner, J., Kozawa, K., Mara, S., Sioutas, C., 2010.
483 Impact of roadside noise barriers on particle size distributions and pollutants
484 concentrations near freeways. *Atmospheric Environment* 44, 3118–3127.
485 <https://doi.org/10.1016/j.atmosenv.2010.05.033>
- 486 Papageorgakis, G.C., Assanis, D.N., 1999. COMPARISON OF LINEAR AND NONLINEAR
487 RNG-BASED k -epsilon MODELS FOR INCOMPRESSIBLE TURBULENT FLOWS.
488 *Numerical Heat Transfer, Part B: Fundamentals* 35, 1–22.
489 <https://doi.org/10.1080/104077999275983>
- 490 Petters, A., von Klot, S., Heier, M., Trentinaglia, I., 2004. Exposure to Traffic and the Onset of
491 Myocardial Infarction. *The New England Journal of Medicine* 351, 1721–1730.
492 <https://doi.org/10.1056/NEJMoa040203>
- 493 Richards, P.J., Norris, S.E., 2011. Appropriate boundary conditions for computational wind
494 engineering models revisited. *Journal of Wind Engineering and Industrial*
495 *Aerodynamics* 99, 257–266. <https://doi.org/10.1016/j.jweia.2010.12.008>
- 496 Roache, P.J., 1994. Perspective: A Method for Uniform Reporting of Grid Refinement Studies.
497 *Journal of Fluids Engineering* 116, 405. <https://doi.org/10.1115/1.2910291>
- 498 Schatzmann, M., Leitl, B., 2011. Issues with validation of urban flow and dispersion CFD
499 models. *Journal of Wind Engineering and Industrial Aerodynamics* 99, 169–186.
500 <https://doi.org/10.1016/j.jweia.2011.01.005>
- 501 Schulte, N., Snyder, M., Isakov, V., Heist, D., Venkatram, A., 2014. Effects of solid barriers
502 on dispersion of roadway emissions. *Atmospheric Environment* 97, 286–295.
503 <https://doi.org/10.1016/j.atmosenv.2014.08.026>
- 504 Tominaga, Y., Stathopoulos, T., 2007. Turbulent Schmidt numbers for CFD analysis with
505 various types of flowfield. *Atmospheric Environment* 41, 8091–8099.
506 <https://doi.org/10.1016/j.atmosenv.2007.06.054>
- 507 United Nations, Department of Economic and Social Affairs, Population Division, 2019. World
508 Urbanization Prospects: The 2018 Revision (ST/ESA/SER.A/420). New York: United
509 Nations.
- 510 Wang, S., Wang, X., 2019. Modeling and Analysis of the Effects of Noise Barrier Shape and
511 Inflow Conditions on Highway Automobiles Emission Dispersion. *Fluids* 4, 151.
512 <https://doi.org/10.3390/fluids4030151>

- 513 Woodward, J.L., 1998. Estimating the flammable mass of a vapor cloud, A CCPS concept book.
514 Center for Chemical Process Safety of the American Institute of Chemical Engineers,
515 New York, N.Y.
- 516 Yakhot, V., Orszag, S.A., Thangam, S., Gatski, T.B., Speziale, C.G., 1992. Development of
517 turbulence models for shear flows by a double expansion technique. *Physics of Fluids*
518 *A: Fluid Dynamics* 4, 1510–1520. <https://doi.org/10.1063/1.858424>
519

Pre-print